Salt Fingers Observed in the Mediterranean Outflow Region (34°N, 11°W) Using a Towed Sensor

BRUCE MAGNELL[1]

Department of Meteorology, Massachusetts Institute of Technology, Cambridge 02139

(Manuscript received 4 November 1975, in revised form 9 February 1976)

ABSTRACT

A towed microstructure instrument has been used to measure small-scale conductivity fluctuations in a quasi-horizontal plane, as well as local vertical gradients of temperature and conductivity. This instrument was towed in the Mediterranean Outflow region (34°N, 11°W) in July 1973, in an area where "step-like" vertical profiles of temperature and salinity had previously been observed. It was found that intense small-scale horizontal structure (1 cycle cm^{-1}) occurred in the thermocline on the thin high-gradient sheets which separated the mixed layers of the step-like structure. Good general agreement between the observed dominant wavelength and amplitude of this structure, and expected theoretical salt finger wavelength and amplitude, strongly suggest that this activity was salt finger convection.

1. Introduction

Salt fingering is purely a local instability, dependent only on the local vertical gradients of temperature and salinity (Stern, 1960; Turner, 1967). This type of double-diffusive convection can be expected to occur at sharp temperature-salinity interfaces in the ocean provided that it is not inhibited by ambient shear, and that the criterion for its onset and maintenance is met, namely, $\alpha\Delta T/\beta\Delta S < (K_T/K_S)^{\frac{1}{2}}$ (Huppert and Manins, 1973), where ΔT and ΔS are the temperature and salinity increments across the sharp interface (positive upward), $\alpha\Delta T$ and $\beta\Delta S$ are the magnitudes of the vertical density increments due to temperature and salinity ($\alpha = \rho_0^{-1}\partial\rho/\partial T$, $\beta = \rho_0^{-1}\partial\rho/\partial S$, where ρ_0 is some reference fluid density), and K_T and K_S are the respective kinematic diffusivities. The latter of these conditions is met nearly everywhere in the main thermocline in the Atlantic Ocean, and in particular on thin sheets of high vertical gradient of temperature and salinity such as those reported by Cooper and Stommel (1968), Tait and Howe (1968, 1971) and Howe and Tait (1970) among others. Consequently, it is of interest to determine whether or not salt fingering convection is actually present on such interfaces. This paper describes an effort to observe fingering *in situ*.

Salt fingering is an ordered phenomenon. Salinity, temperature, density and vertical velocity all exhibit periodic horizontal variations in an ideal field of fingers. This orderliness is their characteristic signature, making them distinguishable against the randomness of other oceanic phenomena. Strictly, in order to prove the existence of fingering it would be necessary to demonstrate the existence of a columnar structure and alternating up-and-down vertical velocity within the columns. But no mechanism other than salt fingering is expected to produce regular horizontal variations of temperature and salinity; thus for practical purposes the existence of any quasi-periodic horizontal variation, localized on a sharp interface, whose wavelength matches approximately the expected salt finger wavelength calculated from the local vertical gradients, is very suggestive of the presence of fingering.

A towed microstructure instrument (TMI) capable of resolving structures of salt finger size was constructed. For engineering reasons electrical conductivity was chosen as the parameter to be measured by the high-resolution probe. Conductivity is a good indicator for salt fingers because it is an increasing function of both temperature and salinity, although it is dynamically irrelevant. Auxiliary instruments, incorporated into the TMI to determine ambient conditions, measured local vertical temperature and salinity gradients, as well as pressure and towing speed. No attempt was made to measure ambient velocity shear.

The TMI was towed in July 1973 in the Atlantic southwest of Gibraltar (referred to hereafter as the Mediterranean Outflow region). Following a brief description of the instrument and its uses, some data from this region are examined.

2. The towed microstructure instrument

a. The vehicle

Since the presence of salt fingers is indicated by their periodic signature in the horizontal, a towed probe was

[1] Present affiliation: EG&G, Environmental Consultants, Waltham, Mass. 02154.

necessary. Thus the TMI was built around a towed "fish," shown in Fig. 1. Its attitude and orientation were controlled by fixed planes at the rear, and it pulled itself downward by means of hydroplanes amidships. It was not streamlined, since towing speeds of 3 kt (150 cm s^{-1}), or less, were planned. In operation, it towed in a slightly nose-down attitude as shown in Fig. 1; however, its attitudinal and directional stability were observed in shallow water trials to be good.

The TMI required about 6000 m of cable out in order to tow at a depth of 1800 m at a speed of 150 cm s^{-1}. Control of the TMI was by varying the speed of the ship, and by reeling cable in or out at the winch.

b. Conductivity sensor

At these towing speeds the necessary centimeter-scale resolution required a sensor of small size whose frequency response extended to several hundred hertz. The conductivity instrument used on the TMI (Fig. 1) was designed to achieve frequency response up to 500 Hz with spatial resolution of less than 1 cm. Absolute accuracy was compromised to achieve this. The probe itself (Fig. 2) was a snout-like object which preceded its own electronics housing as it moved through the water. Conductivity was measured in a small volume of water forward of the probe tip, so that the instrument sampled undisturbed water. The probe was designed and constructed solely to achieve optimum dynamic response; however, this design was distinctly non-optimum for absolute stability of the cell constant with respect to temperature changes, principally because of the elongated shape with its long concentric elements of different materials.

The measurement of electrical conductivity is purely electrical and does not involve thermal diffusion. Hence a conductivity probe can have very fast response provided care is taken to ensure thorough flushing to prevent the formation of a stagnation layer on the probe tip. The TMI probe was designed so that water could be sucked back through the center of it by a pump (Figs. 1 and 2). The volume of the flow had to be made proportional to the speed of the instrument through the water, so as to have adequate flow at higher speeds without degrading the spatial resolution at lower speeds; to accomplish this, a large impeller was mounted at the rear of the fish and driven by the forward motion of the TMI, to turn a constant-displacement pump. The impeller and pump are shown in Fig. 1.

The absolute value of electrical conductivity, and its time derivative, referred to as C_g and C' respectively, were transmitted to the surface ship separately through the FM multiplex transmission system (described below). The C_g signal provided an indication that the instrument was working properly, and also a gross idea of the absolute conductivity structure. The C' signal, being a time-rate-of-change (rolled off above 500 Hz), emphasized the essential high-frequency information to minimize noise introduced in transmission and recording.

The electrical conductivity of sea water is an increasing function of temperature and salinity (after

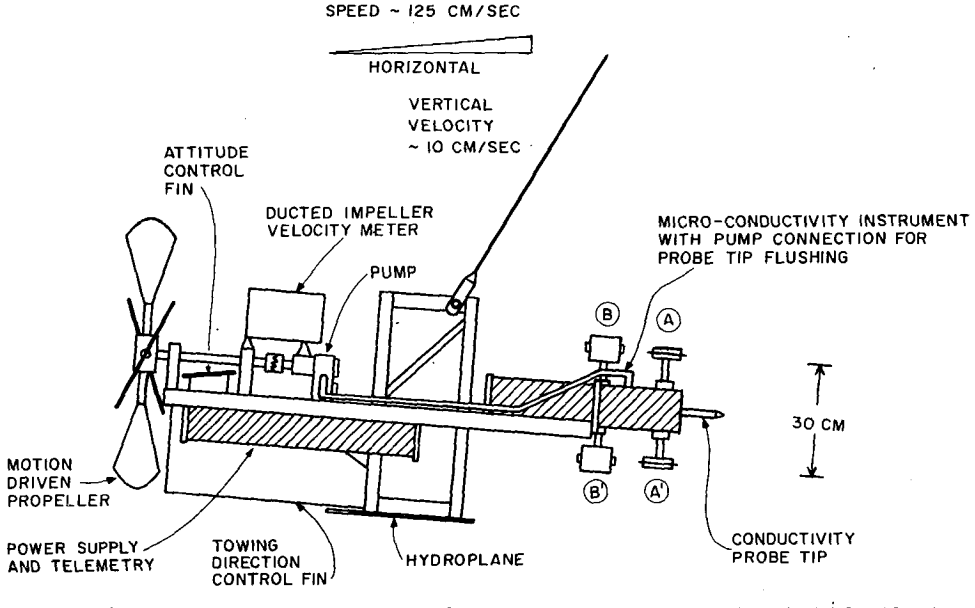

FIG. 1. Simplified illustration of the Towed Microstructure Instrument (TMI). Right-side view, stylized representation, approximately to scale. Not shown: pressure sensor, mounted left side. Partially shown: differential conductivity and temperature sensors, mounted left side. AA′, differential temperature sensor; BB′, differential conductivity sensor.

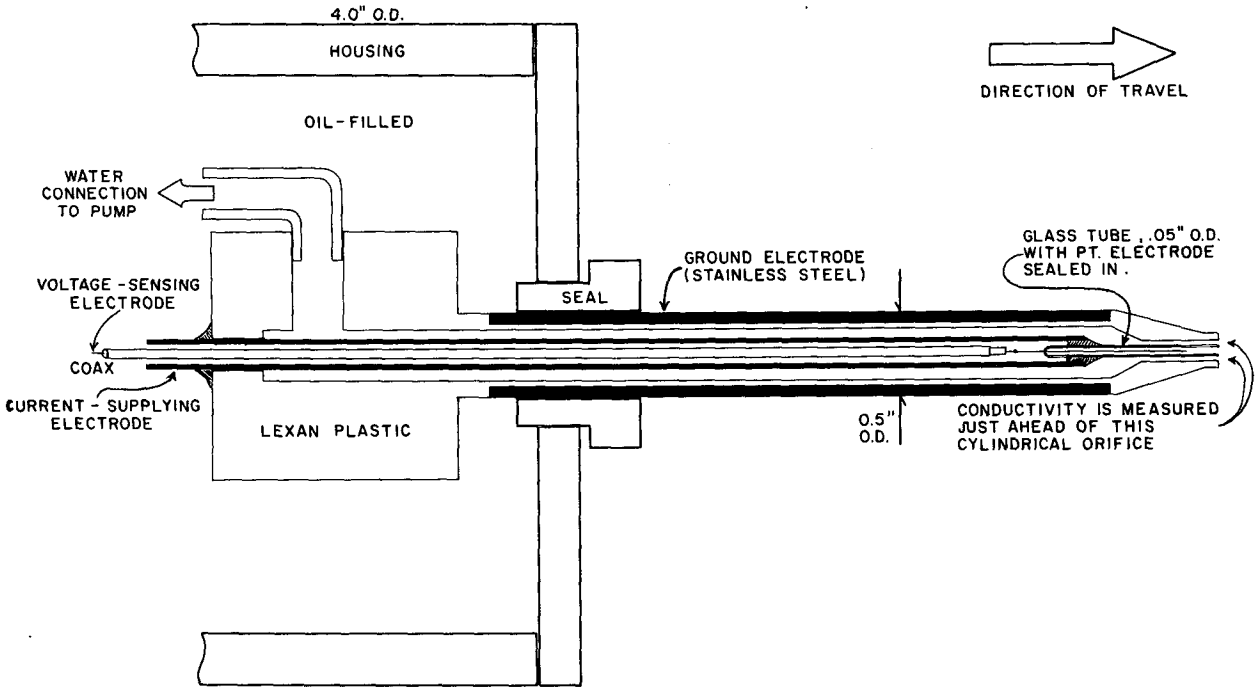

FIG. 2. Detail of conductivity probe sensing element, approximately to scale. Voltage-sensing electrode (innermost), connected to a high-impedance amplifier, draws negligible current. Amplifier output drives current-supplying electrode so as to maintain the ac potential at the probe tip with respect to ground equal to a reference signal.

Riley and Skirrow, 1965), i.e.,

$$\frac{\partial C}{\partial T} = +0.96 \text{ mmho cm}^{-1} (^\circ\text{C})^{-1},$$

$$\frac{\partial C}{\partial S} = +0.99 \text{ mmho cm}^{-1} (‰)^{-1},$$

at $T=15^\circ$C and $S=35‰$. Thus, small conductivity changes (mmho cm^{-1}) are nearly equal to the *numerical* sum of the corresponding changes in temperature and salinity. It is clear that conductivity signals observed in the ocean are mostly due to temperature, since oceanic variability is far greater in terms of °C than in parts per thousand.

c. Other sensors

A pair of vertical differential sensors was incorporated into the TMI (Fig. 1) for the purpose of determining the local vertical gradients of temperature and conductivity. For temperature, a 90-junction thermopile was employed, with the junctions separated vertically by 30 cm. A response time of 150 ms was ensured by placing each junction in a small (0.020 inch diameter) tube exposed to the water. For conductivity, two separate induction-type sensing heads were used, also separated vertically by 30 cm. These two instruments, mounted together on a single housing, were placed aft and to the side of the main conductivity probe on the fish (Fig. 1). By the use of these sensors, it was possible to measure the local 30 cm average vertical differences of temperature (ΔT) and conductivity (ΔC) without regard to whether the TMI was rising, falling, or towing level.

Absolute pressure (Z) was measured with a Bissett-Berman Model 9006 oceanographic pressure sensor. The speed V of the TMI through the water was measured with a ducted impeller (Fig. 1) selected primarily for the constancy of its revolutions per unit distance. This meter was necessary to allow for the conversion of time to distance, since the towing speed could not be held constant. It was not, however, capable of resolving velocity fluctuations on small scales.

d. Telemetry and data recording

The TMI was towed with an electrically-conducting armored cable, with dc power being sent down the cable, and ac telemetry signals sent up. The data channels (C_g, C', ΔC, ΔT, Z, V) were converted to FM form, in proportional bandwidth channels ($\pm 7.5\%$ of center frequency, centered at 2.3, 22.0, 7.35, 3.0, 10.5 and 3.9 kHz, respectively). The FM signals were summed together electronically, and sent up the wire as a complex ac waveform. The FM carrier signals were separated at the surface, and recorded in FM form on an analog tape recorder for later playback and analysis. A stable 5.4 kHz reference frequency was also recorded. Simultaneously, the original signals were

demodulated in real time and displayed on a multichannel strip-chart recorder. This allowed the progress of the experiment to be monitored continuously and altered as necessary to obtain optimum data.

Later, the stored FM data were converted to digital form, using an FM digitizer built at the Massachusetts Institute of Technology. This digitizer consisted of a bank of period counters, controlled by a Nova minicomputer. The clock signal for the counters, 5.4 MHz, was derived from the recorded 5.4 kHz reference signal through a stable phase-lock frequency multiplier. The use of this recorded frequency standard eliminated errors due to tape speed fluctuations.

The digitizer initiated each measurement upon command from the computer. After reset to zero, each counter totalized the clock count for the duration of a selectable number of data cycles, chosen to always fit within the basic measurement repetition rate for that channel. Thus the digitizer measured the period of each data signal averaged over an interval slightly less than the basic measurement repetition interval. Because of the averaging implicit in each measurement, aliasing due to too low a repetition rate could not occur.

3. Results

a. Deployment of the TMI in the region of step-like structure

The TMI was towed on 20 July 1973 during cruise 76 of R/V *Atlantis II*. On this cruise, a survey was made in the Mediterranean Outflow area (Lambert and Evans, 1974) using a high-resolution microprofiling CTD instrument (described by Brown, 1974). Step-like vertical profiles of temperature and salinity, similar to those previously reported in the same area (Tait and Howe, 1968, 1971; Howe and Tait, 1970), were observed in a small region, shown in Fig. 3. Various microstructure-sensing instruments, including the TMI, were then deployed in or through the steps. The tow of the TMI is illustrated in Fig. 3.

The most useful portions of the TMI data consist of several long gradual ascents, during which the rising slope was typically 1:10, as well as a few portions during which the TMI was running level or very gradually descending at slopes less than 1:40. The TMI was caused to rise and sink several times through the depth region between 1300 and 1800 m, where the step-like structure had been found.

The step-like structure found on cruise 76 of the

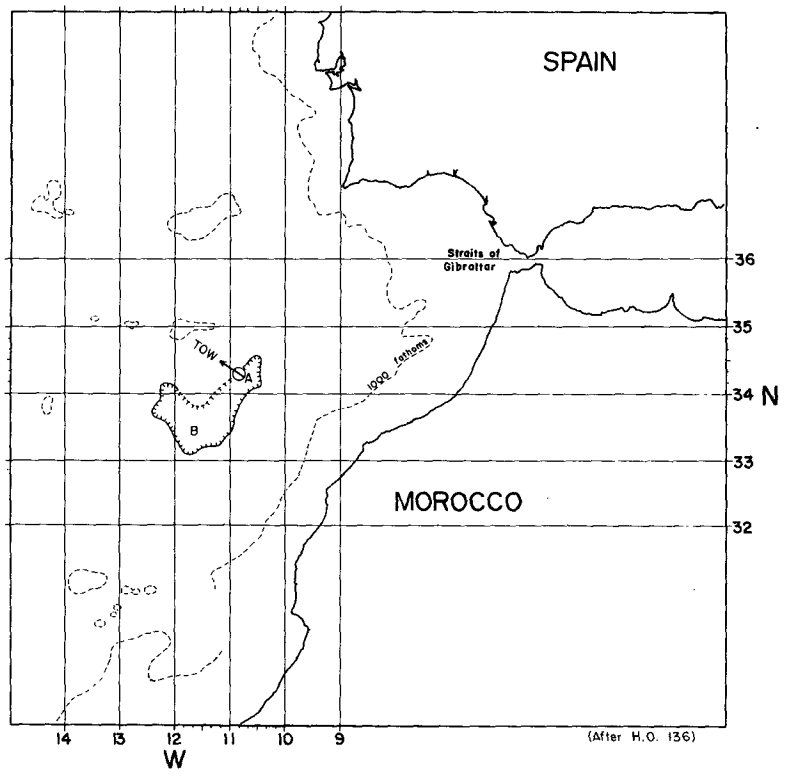

FIG. 3. Chart of Mediterranean Outflow region: A is the region in which step-like vertical profiles were observed during R/V *Atlantis II* cruise 76, July 1973; B is the region in which step-like profiles were reported by Tait and Howe (1971). Tow experiment with TMI (20 July 1973) is indicated by length and direction of arrow.

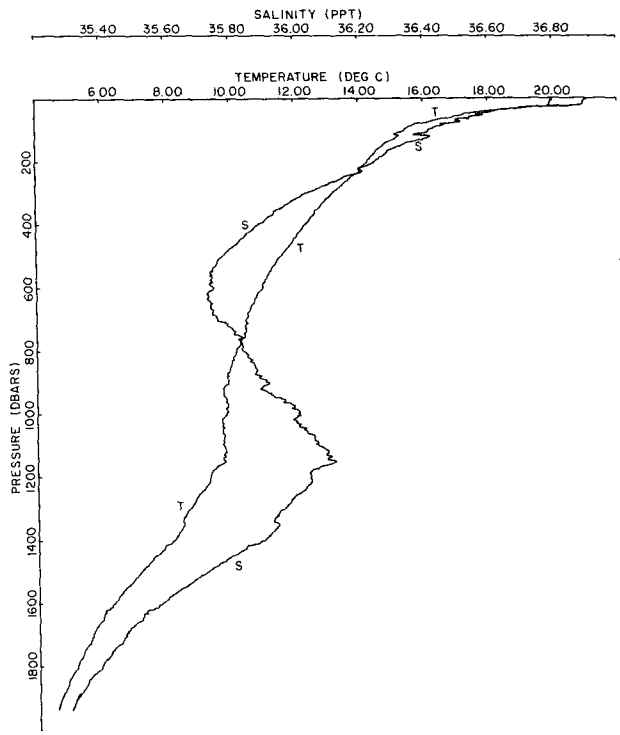

FIG. 4. Profiles of temperature and salinity versus depth. Station 21, lowering 21 (34°15'N, 10°50'W), 1400–1500 GMT 21 July 1973 (after Lambert and Evans, 1975).

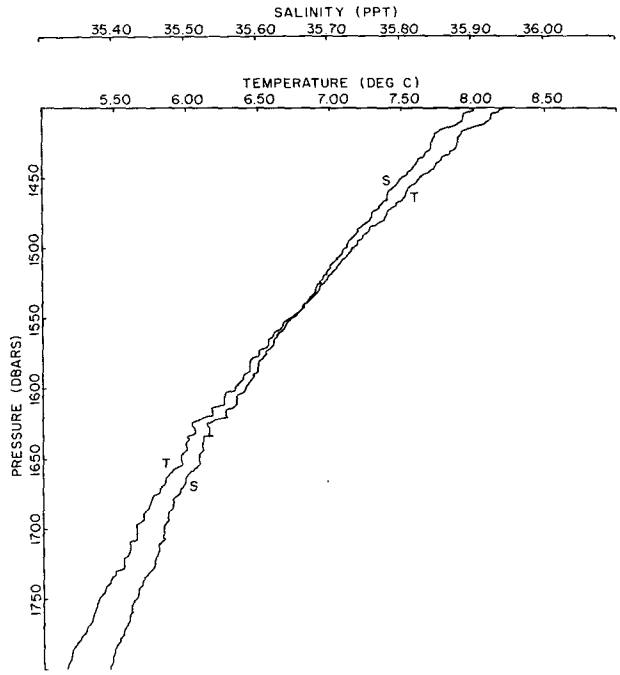

FIG. 5. Enlargement of T-S profiles (from Fig. 4) for lower thermocline region, showing step-like vertical structure.

Atlantis II, reported by Lambert and Evans (1974) and Williams (1974), is illustrated in Figs. 4 and 5 (after Lambert and Evans, 1975, private communication). The temperature and salinity profiles in these figures were taken with the microprofiling CTD instrument at the center of the step region several hours prior to the deployment of the TMI. Fig. 4 shows the large-scale structure, whereas Fig. 5 is an enlargement of the depth region in which the sharpest steps were found.

A typical layer in the steps was about 10 m thick, and a typical interface was less than 1 m thick.

Twenty-two CTD lowerings were made on this cruise in the Mediterranean Outflow region. At each of these stations the step-like structure, if present, was confined to the lower thermocline, although isolated mixed layers were observed at all depths. Two generalizations about the lower thermocline in this area may be made (Lambert and Evans, 1974):

1) Both temperature and salinity decreased monotonically with depth, that is, there were no significant inversions. In particular, salinity always decreased with depth across step-like interfaces; this is a necessary condition for salt fingering to occur.

2) The density ratio across the interface, $\alpha\Delta T/\beta\Delta S$, was always close to unity (a very conservative range would be 1.0 to 1.2).

Moreover, the high-gradient sheets in general, whether or not part of a well-defined staircase, were not markedly more stable than the mean stability in the step-like region; thus, the density profile was proportionately smoother than either the temperature or the salinity

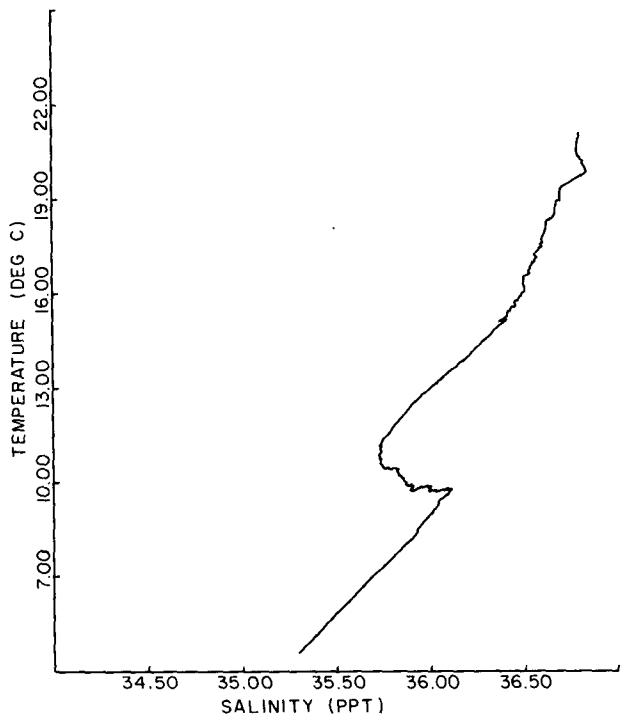

FIG. 6. T-S diagram from Mediterranean Outflow region for location given in legend to Fig. 4.

profile. These facts aid considerably in the interpretation of the TMI data, which was less accurate than the CTD data as to vertical variations in temperature and salinity.

The temperature-salinity plot corresponding to the profiles of Fig. 5 is shown in Fig. 6. The smooth and linear *T-S* relationship for depths greater than that of the salinity maximum gives evidence that Mediterranean water is mixing downward into the North Atlantic Deep Water at the depth of the steps. The *T-S* curve does not indicate where or how the mixing occurs, but in view of its smoothness it is not inconsistent with a local vertical mixing model, such as salt fingers.

b. Description of the TMI data

As the TMI ascended gradually through the ocean, it frequently intersected thin sheets or interfaces having high vertical gradients of temperature and salinity, most often separated by relatively well-mixed regions. Coincident with the passage of the TMI through these interfaces, thin sheets of conductivity microstructure were observed, in the form of intense "bursts" of C' signal (rate-of-change of conductivity), occurring simultaneously with maxima of the local vertical differential temperature (ΔT) and conductivity (ΔC). Fig. 7 illustrates these features, showing a typical 30 min segment of data. The smoothed magnitude of C', denoted $\overline{|C'|}$, is plotted in the lower trace rather than C' itself, to avoid confusion between single spikes and entire bursts, which would otherwise be indistinguishable in the compressed time scale of this figure. The smoothed magnitude $\overline{|C'|}$ is calculated by first band-pass filtering the C' signal in the frequency band 0.16 to 80 Hz, then rectifying and low-pass filtering the result. The low-pass cutoff frequency is 0.5 Hz. This treatment de-emphasizes the occasional narrow spikes which occur frequently in the data but contain little energy. Also shown in Fig. 7 are the 30 cm vertical conductivity difference ΔC_I, as well as the depth and the speed of the TMI. The common time axis advances to the right. During the time interval shown the TMI ascended from a depth of 1720 m to 1425 m at a rate varying from 7.5 to 20 cm s^{-1}, while the speed through the water varied from 55 to 145 cm s^{-1}.

A typical large C' burst, such as the one shown at B in Fig. 7, represents average gradient fluctuations (irrespective of sign) in the plane of motion of the sensor of about 0.007 mmho cm^{-2} (calculated by dividing $\overline{|C'|}$ by the local average speed). By contrast, the peak vertical conductivity gradient for the same event, measured over the 30 cm span, was less than 0.001 mmho cm^{-2}.

The conductivity time-rate-of-change due to motion of the TMI vertically through the observed vertical gradients is buried in the noise level on the C' signal,

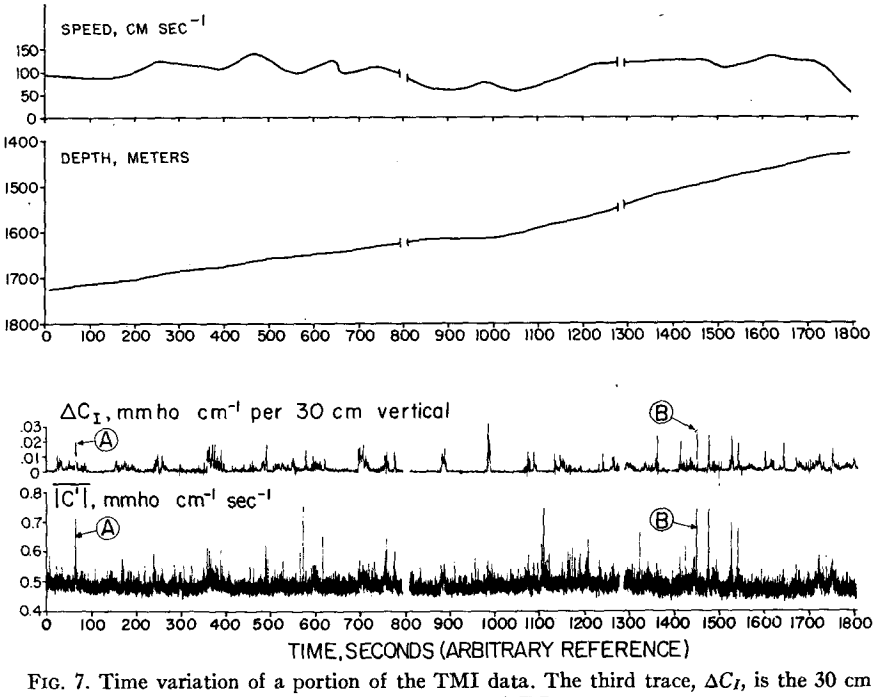

FIG. 7. Time variation of a portion of the TMI data. The third trace, ΔC_I, is the 30 cm vertical conductivity difference, and the lower trace, $\overline{|C'|}$, is the smoothed amplitude of the conductivity time derivative. Momentary malfunctions of the data recording system caused the gaps in the record near the 800 and 1300 s marks.

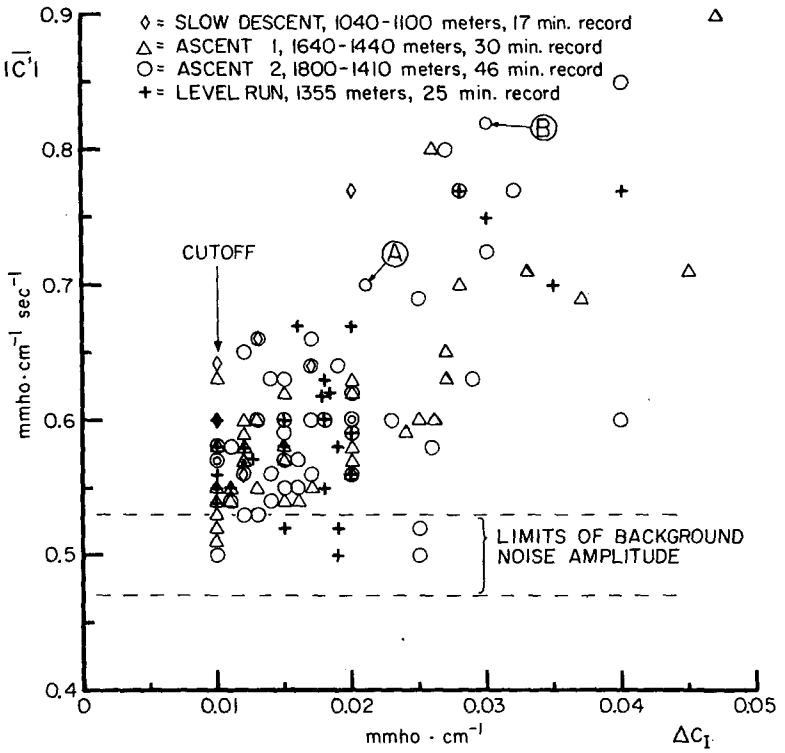

FIG. 8. Peak burst amplitude vs 30 cm vertical conductivity differences. Value of each local maximum of ΔC_I in the time series record, if greater than 0.01 mmho cm^{-1}, is plotted on the abscissa. Smoothed magnitude of C' signal, $\overline{|C'|}$, at the corresponding time is plotted on the ordinate. Points labeled A and B represent events similarly designated in Fig. 7.

as shown by the following calculation:

$$\frac{dC}{dt}=\frac{dC}{dz}\frac{dz}{dt}=(4\times10^{-3}\text{ mmho cm}^{-2})_{\max}$$

$$\times(20\text{ cm s}^{-1})_{\max}=0.08\text{ mmho cm}^{-1}\text{ s}^{-1}.$$

The magnitude of the C' noise level, by comparison, is seen from Fig. 7 to be about 0.5 mmho cm^{-1} s^{-1}. Fig. 7 also demonstrates that the background noise, which is electronically generated, is not a function of the speed of the TMI.

Only a fraction of the total record from the TMI is shown in Fig. 7, but it is representative of the striking correlation between the bursts and the interfaces everywhere in the thermocline. Fig. 8 summarizes the relationship for all the useful data. In this figure the peak 30 cm vertical conductivity difference across every "interface" (local vertical gradient maxima), if greater than 0.01 mmho cm^{-1}, is plotted on the abscissa. The peak amplitude of C' at each corresponding time is plotted on the ordinate. With few exceptions all major interfaces (high ΔC_I) had horizontal microstructure significantly above the noise level. The cutoff at $\Delta C_I=0.01$ was selected to prevent inclusion of numerous minor gradient maxima. Note that Fig. 8 does not address the converse question of whether every burst occurred on an interface, although this was generally found to be true in the thermocline as well.

The methods of analysis for individual bursts, and the general characteristics and implications of the observed bursts, are discussed below. The interface and burst marked A in Figs. 7 and 8 is analyzed in detail in subsequent sections as a typical example of salt fingering.

c. Spectral analysis of burst data

The C' data were treated as a series of independent events, each consisting of the appearance of a transient deterministic signal above continuous background noise. Each event was analyzed separately, with the objectives of determining the signal-to-noise ratio, the presence or absence of a marked periodicity in the signal, and, if such periodicity were present, its amplitude and wavenumber. Comparison of the power density spectrum of each burst with spectra of adjacent background noise was found most useful for this, although inspection of the data in the time domain also aided interpretation.

The spectrum of each burst, as used herein, represents merely a Fourier decomposition of the signal. Because

of the shortness and obvious lack of stationarity of each C' burst, it is not correct to regard the spectrum as a stable estimate of any theoretical salt finger spectrum. By contrast, the background noise appears to be a stationary random process. Although its spectrum could be accurately estimated and bounded with confidence limits, this would be of no interest except insofar as the burst signals rise above it. The peak spectral values (rather than the mean values) from spectra of noise segments adjacent to each burst, made in identically the same manner as each burst spectrum itself, are the most useful quantity for comparison.

To make the spectral computations the C' data were digitized directly from the magnetic tape containing the FM signal using the MIT FM digitizer (described in the instrumentation section). The digitizer produced integrated frequency counts 360 times per second. This rate was found empirically to be high enough to resolve all useful signals; at the typical towing speed of 100 cm s^{-1}, this is equivalent to a spatial resolution of 0.55 cm wavelength.

Power density spectra of C' were computed from the digitized time series for data blocks of variable lengths. The mean was removed and a cosine taper applied to each block before Fourier transformation. Averaging of adjacent points in the frequency domain was performed to bring all spectra to the same approximate resolution bandwidth, 0.71 Hz. Power density values were divided by the square of the quasi-instantaneous velocity (averaged over the data segment length or 2 s, whichever was longer) to convert from the time derivative C' to a spatial derivative, dC/dx. The frequency values were divided by the velocity to convert from frequency (Hz) to wavenumber k (cycles cm^{-1}). Finally the spectra were integrated in wavenumber space by dividing power density values by $(2\pi k)^2$ to convert from units of dC/dx to conductivity fluctuations C. These operations result in smoothed spectra of conductivity fluctuations as a function of wavenumber.

d. General characteristics and implications of bursts

These intense bursts of high-wavenumber gradient fluctuations, whose peak gradients were much higher than the mean 30 cm vertical gradient, were unlikely to have been caused by the passage of the instrument through purely vertical gradients, as this would require a multi-layered structure having numerous temperature and/or salinity inversions on vertical scales of less than 1 cm. The bursts must therefore represent quasi-horizontal variations of conductivity.

The existence of localized intense horizontal microstructure, strongly correlated with vertical gradient maxima, is a central result of this work. It means that nearly all the sharp interfaces have intense activity on them in this part of the ocean.

Forty bursts were subjected to spectral analysis, and all were found to contain conductivity fluctuation energy significantly above the noise level at wavenumbers up to about 1 cycle cm^{-1}. The presence of energy at these high wavenumbers in a horizontal plane indicates that the generating mechanism for this activity on the interfaces must be occurring nearly continuously since such small-scale structures are rapidly destroyed by diffusion.

The wavelength ($\sim$1 cm at the spectral cutoff) of most of the bursts is smaller than the thickness of the interfaces, often by more than an order of magnitude. This implies that the burst is not likely to be an interfacial gravity wave observed directly, since even the shortest such interface wave would have a wavelength several times the interface thickness (Batchelor, 1967).

The bursts might also represent isotropic turbulence caused by shear instability, that is, by the breakdown of a Kelvin–Helmholtz wave. But shear instability would be expected to be far more intermittent than the TMI data indicate.

A local generating mechanism seems to be required to account for the prevalence of the horizontal microstructure, although some of the bursts may of course be due to turbulence. This conclusion does not depend on the details of the bursts, except that they all exhibit energy at high wavenumbers. Salt-finger convection, being a locally-generated activity, is consistent with these conclusions.

e. Detail of salt finger interface

During a gradual ascent, the TMI encountered an interface, marked A on Fig. 7, and a simultaneous burst of horizontal microstructure at a depth of 1725 m. Step-like structure had been previously encountered around this depth on other ascents of the TMI. This interface, however, was isolated and not part of a continuous staircase. It was thin, having a sharp conductivity gradient but a relatively small step change in temperature and salinity. The corresponding burst of microstructure was short and well organized. Fig. 9 shows this burst of C' as a function of time on a highly expanded time scale; individual fluctuations are well resolved. The power density spectrum of conductivity fluctuations versus wavenumber for this burst is shown in Fig. 10. The vertical bars shown in Fig. 10 represent the typical peak-to-peak variations between spectra of four adjacent noise segments at several wavenumbers, these spectra being made in a manner identical to the burst spectrum. The mean of these four spectra is shown by the thinner (inferior) trace.

The speed of the TMI was 87 ± 4 cm s^{-1} at the time of the burst, averaged over a 4 s interval centered on the burst. The vertical velocity was 9 ± 2 cm s^{-1} upward.

Properties of this interface, as measured by the vertical differential sensors, are listed below (interface thickness and gradient values are estimates corrected

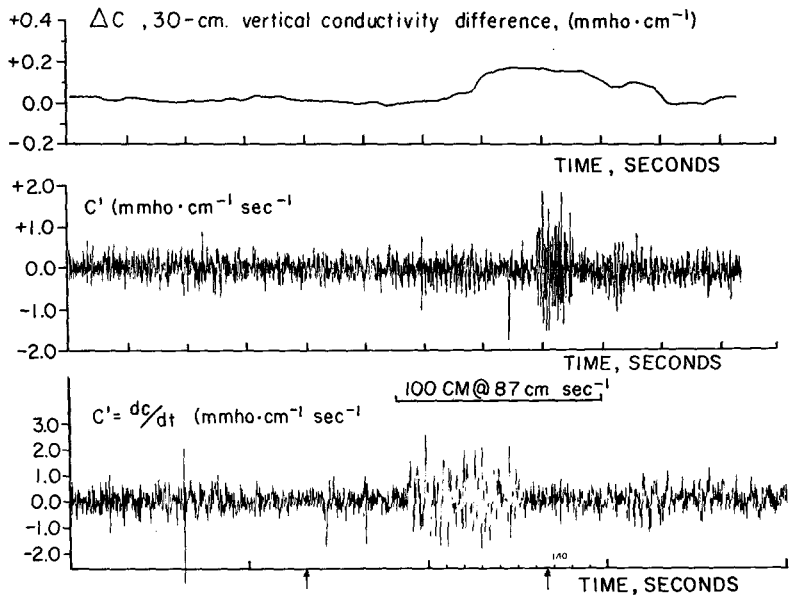

FIG. 9. Salt finger event. This is an expanded time series of the event marked A in Figure 7. The upper trace, ΔC_I, shows the local environment; note, however, that because ΔC_I is the conductivity difference over a finite vertical scale, the peak appears longer in duration than the burst itself. The middle trace shows the burst on the same time scale as the upper trace, and the bottom shows it further expanded in time. The upper and middle traces are analog records; the lower is plotted from digitized data. High-frequency events (sharp spikes in the lower trace) are attenuated in the analog playback. Power density spectrum (Fig. 10) is computed over the block shown between the small vertical arrows. Depth, 1725 m; speed 87 cm s^{-1}; vertical velocity; 9 cm s^{-1}.

for the 30 cm vertical sensor spacing):

ΔZ_I (interface thickness) = 6 cm

ΔT_I (interface temperature step) = 0.021 ± 0.003°C

dT/dz (interface temperature gradient)
$= +3.50 \times 10^{-3}$ °C cm^{-1}

ΔC_I (interface conductivity step)
$= 0.023 \pm 0.002$ mmho cm^{-1}

dC/dz (interface conductivity gradient)
$= 3.83 \times 10^{-3}$ mmho cm^{-2}.

It will be noted that the uncertainty of ΔT_I and ΔC_I, resulting principally from a time-constant mismatch in the sensors, would yield a wide range of salinity step estimates. A conservative range of estimates of S_I is therefore made by assuming the density ratio across the interface, $\alpha\Delta T/\beta\Delta S$, to be between 1.0 and 1.2. Taking $\alpha = \rho_0^{-1}\partial\rho/\partial T = 1.63 \times 10^{-4}$ (°C)$^{-1}$ at 35‰, 7°C, and 1400 db (Sverdrup *et al.*, 1942), and $\beta = \rho_0^{-1}\partial\rho/\partial S = 7.72 \times 10^{-4}$ (‰)$^{-1}$ (Riley and Skirrow, 1965), ΔS_I is

$$0.0037‰ < \Delta S_I < 0.0044‰.$$

This estimate of the salinity step compares well with those observed with the microprofiling CTD (Fig. 5), for correspondingly small temperature steps. The true value is probably close to the upper bound, corresponding to a density ratio near unity.

Inspection of the burst as a function of time (Fig. 9) yields:

Duration = 0.7 s

Number of complete cycles of $C' = 18$

Mean frequency = 25 Hz

Mean wavenumber at 87 cm s^{-1} = 0.29 cycle cm^{-1}

Typical peak-to-peak C' amplitude
$= 2.5$ mmho cm^{-1} s^{-1}

Equivalent amplitude of conductivity fluctuations
= 0.016 mmho cm^{-1}.

The power density spectrum of conductivity fluctuations (Fig. 10) shows a dominant peak centered at 0.24 cycle cm^{-1}, with a bandwidth of 0.08 cycle cm^{-1}. Thus the dominant wavelength is 4.16 cm. The peak-to-peak conductivity fluctuation, integrating all the energy in the peak and correcting for the fact that the segment length used in the analysis was longer than the burst (Fig. 9), is 0.015 mmho cm^{-1}.

f. Comparison of observations with theory

Huppert and Manins (1973) derived an analytical solution to the equations of motion for the case of finite-amplitude salt-finger convection. Their equations can be recast to yield the following formula for the wave-

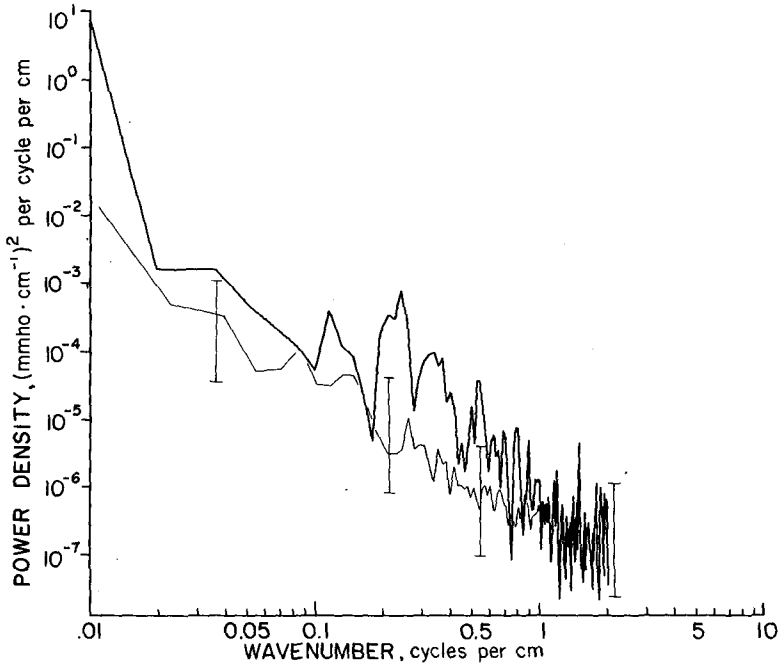

FIG. 10. Power density of conductivity vs wavenumber for the burst shown in Fig. 9. This spectrum is computed by fast Fourier transform over segment of data shown in Fig. 9 between small vertical arrows. It is longer than the burst and thus includes some noise. Allowance for this is made when calculating peak-to-peak conductivity differences from the dominant spectral peak.

length λ of salt-finger convection:

$$\lambda = 2\pi\left[\frac{g\alpha\bar{T}_z}{4\nu K_T}\left(1-\frac{1}{r}\right)\right]^{-\frac{1}{4}},$$

where:

$\bar{T}_z$ local vertical temperature gradient in the fingering region ($+3.50\times10^{-3}$°C cm^{-1} for this interface)

α thermal coefficient of density [$=-1.63\times10^{-4}$ (°C)$^{-1}$]

ν kinematic viscosity [$=1.4\times10^{-2}$ cm^2 s^{-1}]

K_T kinematic thermal diffusivity [$=1.4\times10^{-3}$ cm^2 s^{-1}]

r ratio of flux of buoyancy due to heat to flux of buoyancy due to salt [$=\alpha F_H/\beta F_S$]

F_H net vertical flux of heat due to fingering

F_S net vertical flux of salt due to fingering

g acceleration of gravity [$=980$ g cm s^{-2}].

(Note that λ as here defined is twice the finger diameter.) The value of r has been variously reported on the basis of laboratory experiments to range from 0.56 (Turner, 1967) to 0.1 (Linden, 1973). Using $r=0.56$, the theoretical salt finger wavelength would be $\lambda=4.1$ cm. If $r=0.1$, then the theoretical wavelength would be $\lambda=2.2$ cm.

The observed wavelength of conductivity fluctuations within the previously discussed burst was shown to be $\lambda=4.16$ cm. However, if the burst were salt fingers having a square plan-form, then the actual wavelength defined in a direction parallel to the cell edges would lie between 4.16 cm (if the probe had moved parallel to the cell boundaries) and 2.94 cm (if the probe moved on a diagonal). Within these limits of uncertainty, it is concluded that the observed wavelength agrees with the calculated theoretical wavelength.

The TMI data described only conductivity fluctuations within the burst; temperature and salinity cannot be separated. Hence in order to compare the observed amplitude of fluctuations within the burst with the amplitude predicted from theory, it is necessary to express the theoretical amplitude in terms of equivalent conductivity.

Let ΔT_F and ΔS_F be the vertically averaged temperature and salinity differences between adjacent upgoing and downgoing fingers. Also, assume that up and down velocities within the fingers are equal. Then the ratio r of the vertical flux of buoyancy due to temperature to the flux of buoyancy due to salinity will be (to a first approximation)

$$r=\frac{\alpha F_H}{\beta F_S}\approx\frac{\alpha\Delta T_F}{\beta\Delta S_F}. \qquad (1)$$

This equation establishes a proportion between ΔT_F

and ΔS_F, depending upon the value of r:

$$\Delta T_F = \frac{\beta}{\alpha} r \Delta S_F. \quad (2)$$

Furthermore, as a consequence of the low diffusivity of salt, it is reasonable to suppose that the peak-to-peak salinity difference between fingers is equal to the vertical salinity difference across the interface, ΔS_I. Thus

$$\Delta T_F = \frac{\beta}{\alpha} r \Delta S_I. \quad (3)$$

As discussed previously, the TMI did not produce accurate estimates of vertical salinity differences. Therefore, in order to estimate ΔS_I for the interface in question, it is necessary to assume that the temperature and salinity differences across typical interfaces nearly cancel one another in their effect on density. The basis for this assumption has been discussed previously, and it was shown that a conservative range of variability was found to be

$$1 \leqslant \frac{\alpha \Delta T_I}{\beta \Delta S_I} \leqslant 1.2 \quad (4)$$

or

$$0.83\left(\frac{\alpha}{\beta}\right)\Delta T_I \leqslant \Delta S_I \leqslant \left(\frac{\alpha}{\beta}\right)\Delta T_I. \quad (5)$$

Eliminating $(\beta/\alpha)\Delta S_I$ from (5) and (3) it is found that

$$r(0.83)\Delta T_I \leqslant \Delta T_F \leqslant r \Delta T_I. \quad (6)$$

The conductivity difference (ΔC_F) between fingers is approximately

$$\Delta C_F \approx \Delta T_F + \Delta S_F,$$

which, in terms of ΔT_I, yields

$$\left(r + \frac{\alpha}{\beta}\right)(0.83)\Delta T_I \leqslant \Delta C_F \leqslant \left(r + \frac{\alpha}{\beta}\right)\Delta T_I. \quad (7)$$

The quantity α/β is taken to be 0.21; and r may range as before from 0.1 to 0.56. Inserting the observed ΔT_I of 0.021 ± 0.004°C into (7), the extremes of ΔC_F (mmho cm^{-1}) are calculated to be

$$0.0054 \leqslant \Delta C_F \leqslant 0.016,$$

where the lower bound corresponds to $r=0.1$ and $\Delta T_I = 0.017$°C, and the upper bound corresponds to $r=0.56$ and $\Delta T_I = 0.025$°C.

Although these limits of ΔC_F are believed to be reasonable, many assumptions and simplifications (perhaps unjustified) have been required to obtain them, and no confirming laboratory experiments have been reported.

Since the observed amplitude of conductivity fluctuations within the burst was 0.015 mmho cm^{-1} (peak-to-peak), the agreement between theory and observation is satisfactory, with the best amplitude correspondence being obtained for values of r near Turner's (1967) value of 0.56.

The overall consistency with respect to wavelength and amplitude of these data with theory and laboratory measurements of salt fingers strongly suggests that this particular burst was salt fingers.

g. Similarity of bursts in the thermocline

The interface presented in detail in the preceding section was atypically thin, and the burst of microstructure was correspondingly short. In addition, most of the energy was concentrated in a restricted spectral band around $\lambda = 4$ cm. The temperature step across the interface was relatively small, and although there was a mixed layer above and below, the interface was not part of a well-defined "staircase" structure.

In the preceding section it was demonstrated that this interface apparently contained salt fingers. Most other interfaces in the thermocline also contained high-frequency horizontal activity, as has been shown in Fig. 8, and have a similar vertical structure (with a

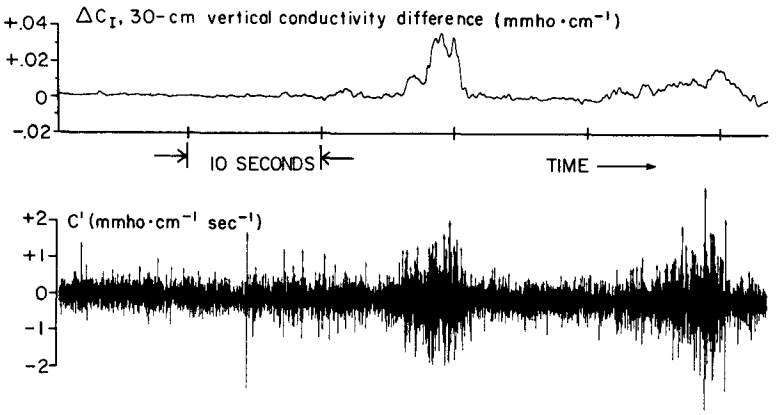

FIG. 11. Example of a longer burst as function of time, from analog record: depth, 1540 m; speed, 140 cm s^{-1}; vertical velocity, 17.5 ± 0.5 cm s^{-1}. This interface is part of a four-step "staircase" structure (other interfaces not fully shown). Burst shown at center of lower trace is expanded in Fig. 12.

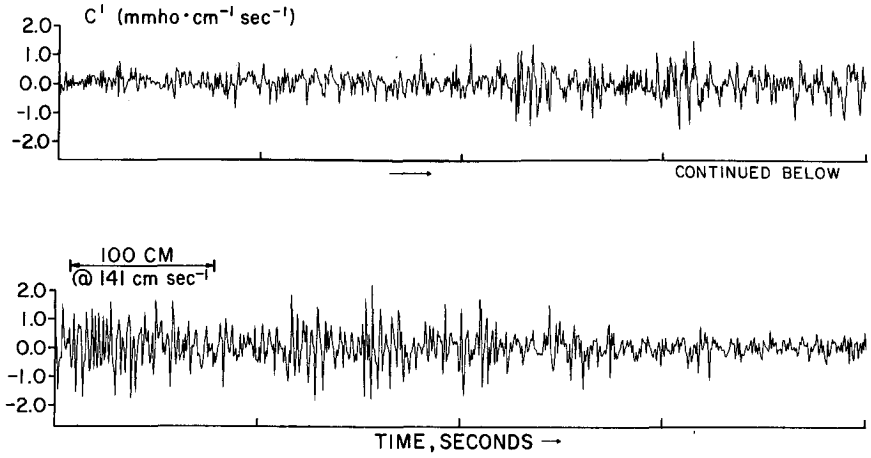

FIG. 12. Detail from Fig. 11, on expanded time scale, plotted from digitized data having higher bandwidth than the analog record of Fig. 11.

destabilizing salinity gradient). Spectral shapes of the various bursts differ mainly in their degree of smoothness; in nearly all cases, the energy in the horizontal gradient is concentrated in the band 6–2 cm, but those bursts which have a longer time record have generally smoother spectra when averaged to the same bandwidth as the shorter ones. However, inspection of the longer bursts as functions of time shows them to be composed of disjoint segments. Each segment may contain roughly three to ten complete cycles. The transition to the next segment may be instantaneous, characterized by a frequency shift, or there may be a gap a few cycles wide in which the amplitude is much reduced. Thus the smoother spectral quality of the longer bursts results mainly from the greater number of segments they incorporate. Laboratory experiments have shown a tendency for salt fingers to form clumps or domains, within which they are well organized, but which have random orientations (Williams, 1975). Such a structure, if traversed by a probe, would give rise to the type of signal observed by the TMI in the longer burst.

An example of a longer burst is shown in Figs. 11 and 12. The interface containing this burst was one of several in a small staircase structure of about four steps.

4. Conclusion

Data gathered with the use of the TMI in the Mediterranean Outflow region 300 mi southwest of Gibraltar in July 1973 strongly suggest the presence of salt finger convection on the numerous temperature and salinity interfaces found in the main thermocline there. Nearly all the sharp interfaces below the depth of the salinity maximum (1100 m), whether part of a well-defined "thermohaline staircase" or not, contained intense high-wavenumber conductivity fluctuations. One such interface in particular has been shown to agree very well with a salt finger model, and the others were generally consistent as well. Vertical gradients of temperature, salinity and density on these interfaces were favorable for salt fingering.

Thus the TMI data, which provide the first *in situ* direct measurements of wavelength and amplitude of oceanic salt fingers, independently confirm the results of Williams (1974), whose data from an optical instrument also indicated the presence of salt fingers on sharp interfaces in the Mediterranean Outflow.

The origin of the step-like layers in this region is speculative, even if the existence of salt fingers on the interfaces is accepted. The data are insufficient to tell whether the fingers cause the layers, or whether the fingers are merely active parasites on interfaces created by another mechanism. It is reasonable to suppose, however, that the fingering activity works, in the ocean as in the laboratory, to maintain the sharpness of the interfaces even as it reduces the temperature and salinity contrast between the layers. So although salt fingering may not be the original cause of the step-like structure, fingering may well be the cause of its prolonged existence, and hence of our ability to observe it.

It would be useful in future work to investigate these salt fingering interfaces in more detail. Shear velocity measurements on the microscale, if feasible, would be particularly useful in determining the parameters governing salt finger convection in the ocean, as well as in calculating net vertical mixing rates.

Acknowledgments. The author is indebted to Prof. Henry Stommel of M.I.T. for his guidance and support on this project. Dr. Richard B. Lambert of the University of Rhode Island has made available data taken with the Neil Brown Microprofiling CTD on cruise 76 of R/V *Atlantis II*. The work was supported by the National Science Foundation under Grant GA-30729 X.

REFERENCES

Batchelor, G. K., 1967: *An Introduction to Fluid Mechanics.* Cambridge University Press, 615 pp.

Brown, N., 1974: A precision CTD microprofiler. *Proc. Intern. Conf. Engineering in the Ocean Environment,* Vol. 2, Catalog No. 74 CH 0873-0 OCC IEEE, New York, N.Y. 10017, 270–278.

Cooper, J. W., and H. M. Stommel, 1968: Regularly spaced steps in the main thermocline near Bermuda. *J. Geophys. Res.*, **73**, 5849–5854.

Howe, M. R., and R. I. Tait, 1970: Further observations of thermocline stratification in the deep ocean. *Deep-Sea Res.*, **17**, 963–972.

Huppert, H. E., and P. C. Manins, 1973: Limiting conditions for salt fingering at an interface, *Deep-Sea Res.*, **20**, 315–323.

Lambert, R. B., and D. L. Evans, 1974: A confined thermohaline staircase. *Trans. Amer. Geophys. Union,* **55**, 296 (abstract).

——, and D. L. Evans, 1975: Profiles of temperature and salinity in the Mediterranean Outflow region from cruise 76, R/V *Atlantis II.* (Unpublished.)

Linden, P. F., 1973: On the structure of salt fingers. *Deep-Sea Res.*, **20**, 325–340.

Riley, J. P. and G. Skirrow, 1965: *Chemical Oceanography,* Vol. 1. Academic Press, 712 pp.

Stern, M. E., 1960: The "salt fountain" and thermohaline convection. *Tellus,* **12**, 172–175.

Sverdrup, H. U., M. W. Johnson and R. H. Fleming, 1942: *The Oceans, Their Physics, Chemistry, and General Biology.* Prentice-Hall, 1087 pp.

Tait, R. I., and M. R. Howe, 1968: Some observations of thermohaline stratification in the deep ocean. *Deep-Sea Res.*, **15**, 275–280.

——, and ——, 1971: Thermohaline staircase. *Nature,* **231**, 178–179.

Turner, J. S., 1967: Salt fingers across a density interface. *Deep-Sea Res.*, **14**, 599–611.

Williams, A. J., 1974: Salt fingers observed in the Mediterranean outflow. *Science,* **185**, 941–943.

——, 1975: Images of ocean microstructure. *Deep-Sea Res.*, **22** (in press).